Snapshots of Ce_{70} toroid assembly from solids and solution

Ian Colliard,[1] Jessica C. Brown,[1] Dylan B. Fast,[1] A. Kirstin Sockwell,[2] Amy E. Hixon,[2] and May Nyman[1*]

[1]Department of Chemistry, Oregon State University, Corvallis, OR 97331, USA
[2]Department of Civil and Environmental Engineering and Earth Sciences, University of Notre Dame, Notre Dame, IN 46556, USA

*correspondence: may.nyman@oregonstate.edu

Abstract

Crystallization at the solid-liquid interface is difficult to spectroscopically observe and therefore challenging to understand and ultimately control at the molecular level. The Ce_{70}-torroid formulated $[Ce^{IV}_{70}(OH)_{36}(O)_{64}(SO_4)_{60}(H_2O)_{10}]^{4-}$, part of a larger emerging family of M^{IV}_{70}-materials (M=Zr, U, Ce), presents such an opportunity. We have elucidated assembly mechanisms by X-ray scattering (small-angle scattering and total scattering) of solutions and solids, as well as crystallizing and identifying fragments of Ce_{70} by single-crystal X-ray diffraction. Fragments show evidence for templated growth (Ce_5, $[Ce_5(O)_3(SO_4)_{12}]^{10-}$) and modular assembly from hexamer (Ce_6) building units (Ce_{13}, $[Ce_{13}(OH)_6(O)_{12}(SO_4)_{14}(H_2O)_{14}]^{6-}$ and Ce_{62}, $[Ce_{62}(OH)_{30}(O)_{58}(SO_4)_{58}]^{14-}$). Ce_{62}, an almost complete ring, precipitates instantaneously in the presence of ammonium cations as two torqued arcs that interlock by hydrogen boding through NH_4^+, which can also be replaced by other cations, demonstrated with Ce^{III}. Room temperature rapid assembly of both Ce_{70} and Ce_{62}, respectively, by addition of Li^+ and NH_4^+, along with ion-exchange and redox behavior, invite exploitation of this emerging material family in environmental and energy applications.

Introduction

A molecular building block approach is an important strategy to assemble bioinorganic, hybrid, and inorganic materials. It provides a level of control that is achievable in organic, hybrid organic-inorganic, and bioinorganic synthesis; but is still emerging in purely inorganic synthesis. Rational bottoms-up design has been used to create DNA-nanostructures,[1-2] peptide-nanostructures,[3-4] inorganic macrocycles,[5-9] metal-organic frameworks (MOFs),[10-11] and metal-organic polyhedra.[12] Metal-oxo clusters (including polyoxometalates, POMs), which can be viewed as molecular metal-oxides, have greatly aided our ability to design purely inorganic materials with molecular-level precision. Such synthetic approaches are essential for optimizing materials function, including catalysis,[13] magnetism,[14-18] and luminescence.[19-20] Building-block synthetic approaches have been hypothesized in metal-oxo systems including; 1) assembly of Pd_{84} and Pd_{72} Pd-oxo toroids from a Pd_6 fragment;[21-23] 2) Mn_{84} and Mn_{70} built from a Mn_{12} oxo-acetate;[24-25] 3) growth of giant molybdate POMs from smaller clusters;[26-27] 4) assembly of successively larger Ln_x species (x =

12-140) from a Ln_4 oxocluster building unit;[18, 28-31], 5) isolation of various sized Ln_xNi_y-oxoclusters (up to 164 metal polyhedra) from smaller oxocluster building blocks,[15, 32-33] and 6) capping and linking of POMs into rigid chains and frameworks, and flexible polymers.[34-36]

The d-block and f-block tetravalent metal cations (M^{IV}=Zr/Hf/Ce/U/Np/Pu^{IV}) are amongst the most studied metal-oxo cluster families. Of special note, Zr/Hf MOFs are built of the $M_6(OH,O)_8$ hexamer (M_6), and these MOFs are widely exploited for virtually every application that has been developed to date including catalysis and separations.[37] The M_6 cluster is contained within most M^{IV}-oxoclusters, as well as in fluorite-type MO_2; but it is not possible to simply build MO_2 (and intermediate size clusters such as M_{38}[38-44]) from M_6-units, since the M_6-units share M_2 edges in the larger assemblies. In fact, M_6 is shown to co-exist in solution with monomers, dimers and hexamers,[45-46] likely in dynamic equilibrium. This demonstrates that models of metal-oxo cluster building block approaches such as M_6 → [intermediates] → MO_2 are oversimplified; and ultimately, scientists still lack control over the assembly processes in the M^{IV}-oxocluster families.

Gaining importance and attention is the Ce-oxo clusters, as molecular models of nano-CeO_x catalysts, as well as functional catalysts themselves. The $Ce^{III/IV}$ redox activity distinguishes this family of metal-oxo clusters: Ce_{10}, Ce_{22}, and Ce_{40} oxoclusters have distinct Ce^{III} and Ce^{IV} sites,[44, 47] while Ce_{38} reports mixed $Ce^{III/IV}$-sites.[48] The $M^{IV}{}_{70}$ sulfate ring structure, originally described for $U^{IV}{}_{70}$, followed by $Ce^{IV}{}_{70}$ and Zr_{70},[49-52] is the only M^{IV}-topology besides M_6 that spans transition metals, lanthanides, and actinides, and is also the largest. The hexamer units are distinct in M_{70}, alternating with monomers around the ring (**figure 1a**). This unique arrangement presents an opportunity to study building-block assembly mechanisms. Ce_{70} and U_{70} have thus far been crystallized with mild hydrothermal heating. The transition metals and lanthanides that serve as counter-cations and also link the rings into intricate frameworks probably necessitate the heating to promote complete dissolution.[49-51] In fact, Zr_{70} has been isolated at room temperature, as either a neutral form with no counter-cations or as a Na-salt,[52] supporting this hypothesis. The neutral cluster also challenges our understanding of the role of the counter-cations.

We present here two strategies to capture incomplete fragments of the Ce_{70}-toroid that elucidate assembly pathways. The first strategy is to increase the heterometal (counter-cation) concentration in solution to inhibit full-ring formation. The second strategy is the use of ammonium counter-cations, which promotes extremely rapid assembly of nearly complete Ce_{62}-rings. Three Ce_{70}-fragments are observed by single crystal X-ray diffraction (SCXRD) including Ce_5, Ce_{13}, and Ce_{62} (**figure 1**). Pairs of torqued Ce_{62} open rings mutually stabilize each other by interlocking via H-bonding to ammonium, and X-ray scattering studies show this fascinating interlocking supra-structure assembles immediately at room temperature. Ce^{III} added during the crystallization process replaces the ammonium, connecting the incomplete rings. The Ce_5-fragment, based on its position just above and below the center of the complete Ce_{70}-ring, indicates templating ring growth from smaller fragments, similar to the templating of Mo_{150} wheel from Mo_{36}.[53] On the other hand, Ce_{13} and Ce_{62} indicate the Ce_{70}-ring forms by a building block approach, where building block and templating mechanisms are by no means mutually exclusive.

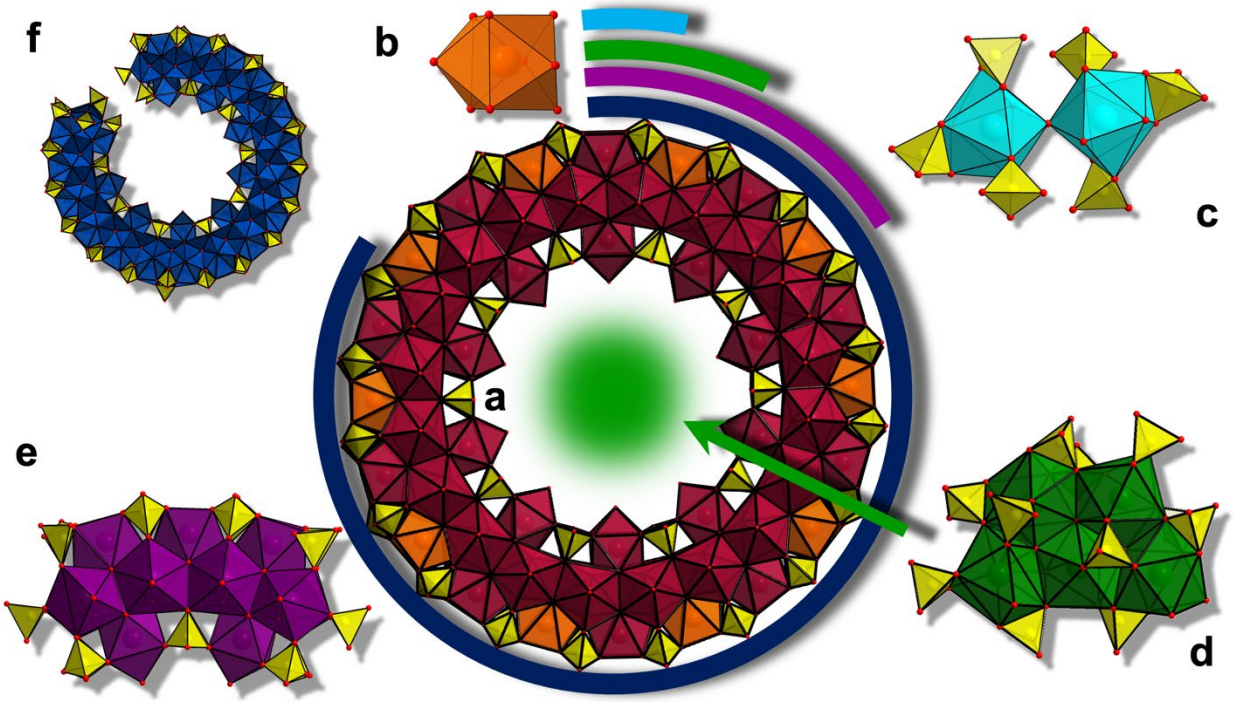

Figure 1. Schematic showing isolated fragments of the **Ce_{70}** ring (**a**). **b**) monomer, $[Ce(H_2O)_9]^{3+/4+}$, **c**) oxo-bridged dimer $[Ce_2^{IV}\text{-}O(SO_4)_4]$, **d**) $[Ce_5O_3(SO_4)_{12}]^{10-}$ pentamer that serves as a template, **e**) $[Ce_{13}(OH)_6(O)_{12}(SO_4)_{14}]^{6-}$, **f)** $[Ce_{62}(OH)_{30}(O)_{58}(SO_4)_{58}]^{14-}$.

Finally, we track room-temperature, *in-situ* assembly via small-angle X-ray scattering (SAXS) of $Ce(SO_4)_2$-$LiNO_3$ solutions. SAXS indicates that addition of Li^+ promotes Ce_{70} formation, but assembly of rings and crystallization as a solid is likely nearly simultaneous. Ultimately Ce_{70} crystallizes out of this *in-situ* study, confirming the observed solution species. This differs from classic POM or aluminum polycation[54-57] systems in which pH is clearly the driver of solution phase assembly while counterions promote crystallization: two distinct roles. In this system, the counter-cation is the driver of simultaneous assembly and crystallization, highlighting the importance of this often-overlooked parameter in prescribing aqueous inorganic reaction mechanisms.[58] In one final structure, we show that lanthanides (Yb^{3+}) can also serve as counterions and framework builders for the Ce_{70}-ring, and the entire family of Ce_{70} and Ce_{62} materials readily undergo cation exchange.

Results and Discussions

All tetravalent metal cations complex water molecules upon dissolution and exhibit strong hydrolysis tendencies. Oligomer formation due to hydrolysis and condensation reactions occur even in acidic conditions,[59] and is accelerated with heat or addition of base. If uncontrolled, this process leads to metal oxide precipitation. The addition of heterometal cations and strongly coordinating oxoanion ligands can compete with the fundamental hydrolysis, olation, and oxolation reactions that drive oligomerization. Most crystalline phases reported here were obtained from $Ce^{IV}(SO_4)_2$ solutions with added ammonium, Ni^{2+} or Yb^{3+}, heated at 75 °C. The exception is the Li^+ salt of Ce_{70}, obtained at room temperature. Details of syntheses are summarized in the SI.

Ce_{70}, $[Ce^{IV}_{70}(OH)_{36}(O)_{64}(SO_4)_{60}]^{4-}$, was described prior, and is also isostructural with Zr_{70} and U_{70}.[49-52] Briefly, the Ce_{70} cluster can be viewed as ten Ce_6-hexamers that alternate with ten Ce_1-monomers. Four sulfates bridge each Ce_6 and Ce_1 along the outer rim, and four additional sulfates bridge only Ce_6 units along the inner rim. Each fragment discussed later can be viewed in the same context. The Ce_{62}, $[Ce_{62}(OH)_{30}(O)_{58}(SO_4)_{58}]^{14-}$, consisting of ~90% of the ring, contains nine Ce_6 and eight Ce_1. Ce_{13}, $[Ce_{13}(OH)_6(O)_{12}(SO_4)_{14}(H_2O)_{14}]^{6-}$, consists of two Ce_6 and Ce_1, and is approximately 20% of the ring. Ce_5 $[Ce_5(O)_3(SO_4)_{12}]^{10-}$, resembles half of the Ce_6 plus two flanking monomers. These clusters and their intrinsic relation to the Ce_{70}, summarized in **figure 1**, serve as crystallographic snapshots of mechanistic pathways for ring formation.

NiCe$_{70}$-PacMan & the Ce$_{13}$ fragment

Prior, we obtained a Ni-linked Ce_{70} framework from a solution of ~2:1 Ce:Ni. In the prior study of TM-linked Ce_{70} (TM=transition metal) frameworks, we observed a general trend of increasing TM concentration in reaction solutions yielded frameworks with more incorporation of Ce-monomers, *instead* of the TM-linkers.[51] This result was initially counterintuitive, but attributable to the TMs inhibiting or slowing Ce_{70} formation. The Ce-monomers are important in these frameworks because they are either mixed $Ce^{III/IV}$ or purely Ce^{III} oxidation state, where both oxidation states were shown to be redox active in the monomer form. Here, increasing the Ni:Ce

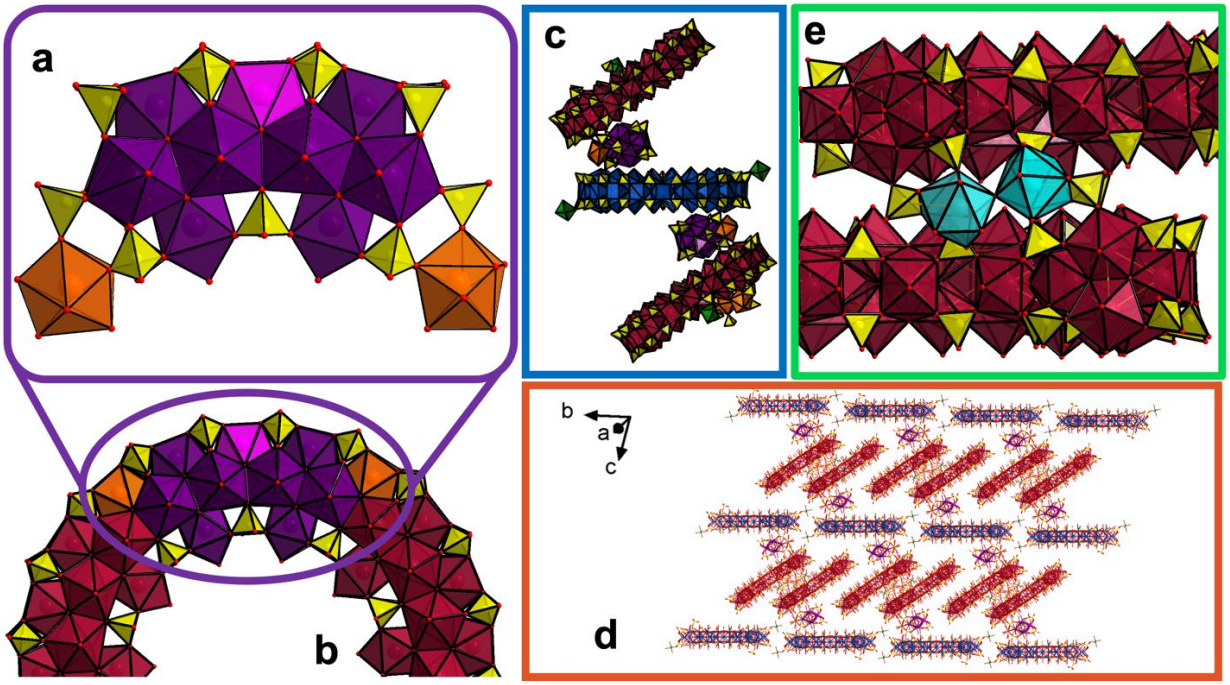

Figure 2. Polyhedral representation of a) Ce_{13} fragment as crystallized in the NiCe$_{70}$PacMan, Ce_{13} can be described as two Ce_6 in purple and the linking monomer in pink, the neighboring sulfate bridged Ce^{III}-monomers are shown in orange. b) The relation of the Ce_{13} and surrounding monomers to the Ce_{70} ring, showing that Ce_{13} is a fragment and in potential stepwise growth. c) The entire building unit of the NiCe$_{70}$PacMan framework, Ni in green, sulfates in yellow, addenda sulfates omitted for clarity, sandwiched Ce_{70} in blue, and terminal Ce_{70} in red. d) Wireframe representation of extended stacking of the $[(Ce_{13})_2Ce_{70}(Ce_{70})_2]$-unit. e) $[Ce_2^{III}\text{-}O]$ dimer in light blue bridging two Ce_{70}.

ratio to almost 1:1, we obtained the **NiCe$_{70}$-PacMan** phase (triclinic space group *P*-1, V = 63,794 (9) Å^3, **table S1**) that features the Ce$_{13}$-fragment (**figure 2**, see SI for synthesis details). **NiCe$_{70}$-PacMan**, named for the resemblance of the Ce$_{70}$-Ce$_{13}$-Ce$_{70}$ unit to the 1980's video game character (**figure 2c**), is described by the moiety formula $[Ni(H_2O)_6]_2$ μ-$[(Ni(H_2O)_5)(Ce(H_2O)_{5.5})_2(Ce_{13}(OH)_6(O)_{12}(SO_4)_{14}(H_2O)_{14})]_2$ $Ce_{70}(OH)_{36}(O)_{64}(SO_4)_{60}(H_2O)_{45}$ μ-$[(Ce^{IV}{}_2$-$O(SO_4)_4(H_2O)_8]$-$[NiCe^{III}{}_{1.5}Ce_{70}(OH)_{36}(O)_{64}(SO_4)_{61.75}(H_2O)_{44}]_2$. The framework is shown in **figure 2d**. Along the *b*-direction, there are approximate layers of Ce$_{70}$ rings (blue). The layers alternate with stacks of offset Ce$_{70}$, tilted from the former layers by ~30º (red). The latter Ce$_{70}$-rings are dimerized, linked by an unusual linear $Ce^{IV}{}_2$-O dimer unit (**figure 2e**). The linear unit (Ce-O-Ce angle = 179.99(6)°) resembles a recently described Pu-O-Pu dimer isolated as a nitrate salt, highlighting a similarity between these f-block elements.[60] Of the $[Ce_{70}]_2$-dimer, one forms the Ce$_{13}$-'pacman' unit with Ce$_{70}$ of the layer above, and the second with the layer below. All Ce$_{70}$ rings present the same core formula as above.

The Ce$_{13}$ fragment is of particular note because it provides a snapshot of the stepwise assembly pathway for the formation of the Ce$_{70}$ ring, as illustrated in **figure 2a,b**. The fragment consists of two hexamers with a bridging monomer, in the exact arrangement observed in Ce$_{70}$. Bond valence analysis (BVA) of the Ce and O for the fragment confirms the overall formula of $[Ce_{13}(OH)_6(O)_{12}(SO_4)_{14}(H_2O)_{14}]^{6-}$ with all Ce^{IV} (**table S11,12**), also identical to Ce$_{70}$. Additionally, the fragment is capped on either side by Ce-monomers which are Ce^{III} (**figure 2a, table S15**). While the Ni^{II} concentration of the reaction solution appears to play a role in isolation of the Ce$_{13}$-fragment, it is very sparse in the isolated framework. All three crystallographically-

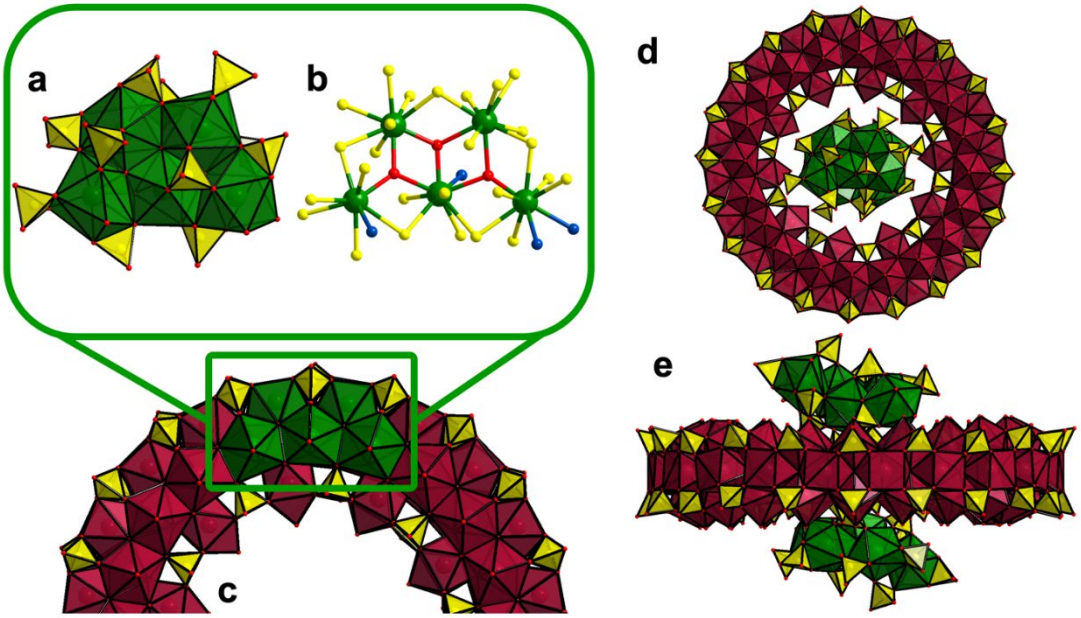

Figure 3. a) Polyhedral representation of Ce$_5$ and b) ball and stick representation of Ce$_5$ cluster with the Ce in green, μ$_3$-oxos in red, oxygens from sulfates in yellow, and aqua oxygens in blue. c) Polyhedral representation of Ce$_5$ in relation to the Ce$_{70}$, d) top view showing the location of the Ce$_5$ in the inner void of the Ce$_{70}$, and e) side showing the location of the Ce$_5$ in the inner void sandwiching a Ce$_{70}$, ammoniums omitted for clarity.

unique Ni^{II} sites are regular $Ni(H_2O)_5(O\text{-}SO_3)$ or $Ni(H_2O)_6$ octahedra decorating the Ce_{70} rings (green polyhedra/spheres in **figures 2c/d**) with bond lengths from 1.98-2.03 (2) Å (BVS=2.1-2.2; see **table S9, S13**). The abundant Ni^{II} in the reaction solution is the most likely reagent for the Ce^{IV} to Ce^{III} reduction, even though all nickel present in the structure is divalent.

Ammonium counterions for fragment isolation.

Ammonium counterions are complex and unpredictable. They are both a weak acid and a weak base. They have a larger effective radius than TM or Ln cations, and are unable to directly bind directly to sulfate.[61] However, they can undergo strong H-bonding in solution and in solids. In our experience, ammonium salts of metal oxo clusters (i.e., polyoxometalates) can be either very soluble or very insoluble, depending on the charge of the cluster. The synthesis of Ce^{IV}-SO_4^{2-}-NH_4^+ compounds reported here differs from the analogous TM or lanthanide Ce^{IV}-SO_4 reactions. Namely, with TM (i.e., **$NiCe_{70}$-PacMan**) or lanthanides (discussed below), the reaction solutions go into the oven completely dissolved, and the Ce_{70}-frameworks crystallize during the 75 °C hydrothermal treatment. The analogous ammonium reaction solutions precipitate immediately upon preparation at room temperature (amorphous precipitate, discussed below), then redissolves upon heating, and come out of the 75 °C oven completely dissolved. The lattices crystallize only upon cooling to room temperature, over the course of a day. The ammonium reactions have yielded several crystal structures, precipitates, and solutions that provide further insight into assembly pathways.

First, a minor co-crystallite, **$NH_4(Ce_5)_2Ce_{70}$**, fully formulated $(NH_4)_{52}[Ce_5(O)_3(SO_4)_{12}(H_2O)_4]_2Ce_{70}(OH)_{36}(O)_{64}(SO_4)_{74}(H_2O)_{36}$, crystallizes in the monoclinic space group *I*2/*a* (V = 74,657 (1) $Å^3$, **table S2**). With no linking TM or $Ce^{III/IV}$ monomers, the Ce_{70} rings are not connected into extended frameworks. However, the Ce_{70} rings are sandwiched between two Ce_5 fragments, which sit just above and below the center of the wheel in a manner that implies templating.

The Ce_5 cluster is formulated as $[Ce_5(O)_3(SO_4)_{12}(H_2O)_4]^{10-}$. The five Ce-centers are assembled in a nearly-planar trapezoidal shape with three bridging oxos between the three centers, shown in red in **figure 3a,b**. Each Ce is 8-9 coordinate, and the remainder of the coordination sphere is completed with bridging and chelating sulfates; no hydroxides are recognized in this unit. BVA of the pentamer confirms a tetravalent charge for these Ce (**table S16)**. The pentameric units cap the inner diameter of the rings, bridged by ammonium hydrogen bonding, with distances ~2.7-3.2 Å. Although we can recognize exactly this pentamer fragment in the Ce_{70}-ring (**figure 3c**), especially the arrangement of the oxo-units, we are biased to think the hexamer and monomer units are the modular building units for Ce_{70} (as well as the U^{IV} and Zr^{IV} analogues). This bias stems from the numerous structures featuring the $[M^{IV}{}_6O_4(OH)_4]$ core for M=Zr, Hf, Ce, Th, U, Np, and Pu.

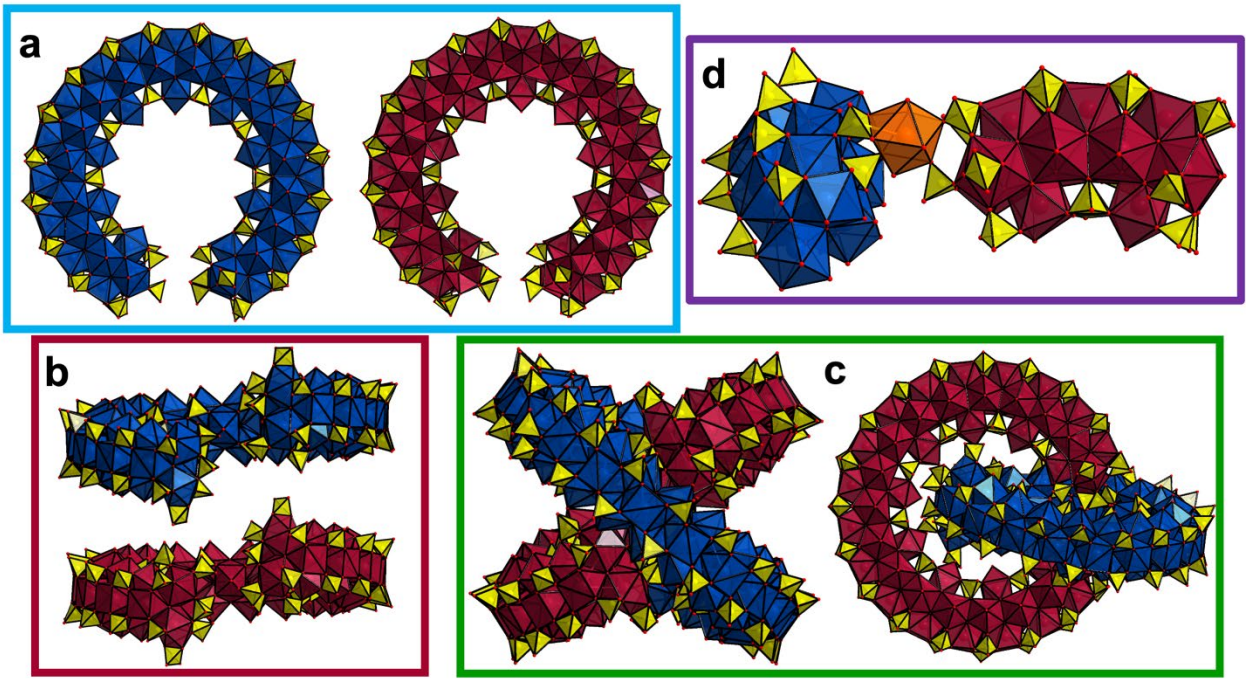

Figure 4. Polyhedral representation of a) top view of the two crystallographically unique Ce_{62} shown in blue and maroon, b) side view of the two unique Ce_{62} showing the ends misaligned, c) side view and top view of the $[Ce_{62}]_2$-dimer d) incorporation of the Ce^{III}-monomer in orange at the end of a Ce_{62} in red coordinating partway the blue Ce_{62}, sulfate in yellow, addenda sulfate and ammoniums omitted for clarity and oxygens in red.

Isolation of this fragment provides two additional hypotheses concerning assembly pathways of M^{IV}-sulfate systems. Missing from this fragment is hydroxyl bridges; most hexamer units alternate oxo and hydroxyl bridges. Generally, oxo vs. hydroxyl bridges can be related to the solution pH and/or acidity of M^{IV}. This suggests it forms during early assembly steps, when pH is highest (protons are released during hydrolysis-condensation reactions), then $M_6O_4(OH)_4$ units form later in the reaction pathway. If our initial hypothesis is correct and the hexamer unit is the main building block, then this pentamer is a 'reject' of the dominant Ce_{70} assembly pathway. The juxtaposition of Ce_5 to Ce_{70} in the crystalline lattice could imply templating of Ce_{70} by smaller units, or alternatively, adventitious siting of Ce_5 on the Ce_{70} face during crystal formation (**figure 3d,e**).

Crystallization of the various ammonium-supported structures is dictated by NH_4^+-concentration. Crystal formation of $\mathbf{NH_4(Ce_{62})_2}$ (described below) occurred at a Ce:NH_4^+ molar ratio range of ~1:20-1:30. No crystal growth is observed at ratios lower than 1:20, and ammonium cerium sulfate monomer salt crystallized at ratios higher than 1:30. The $\mathbf{NH_4(Ce_{62})_2}$ is the only structure that can be obtained as a relatively pure phase at ~1:25 ratio, with $\mathbf{NH_4(Ce_5)_2Ce_{70}}$ (described above) co-crystallizing at a ~1:20 ratio and the $\mathbf{NH_4Ce_{70}}$ co-crystallizing at ~1:30. This indicates the interlocked Ce_{62} rings are quite stable, and stabilized by ammonium since they are not observed with any other counter-cation. Varying reaction conditions and reagents to isolate

pure phases for **$NH_4(Ce_5)_2Ce_{70}$** and **NH_4Ce_{70}** were not successful: **$NH_4(Ce_{62})_2$** was always the most prominent phase.

$NH_4(Ce_{62})_2$, formulated as $(NH_4)_{82}(Ce_{62}(OH)_{30}(O)_{58}(SO_4)_{71}(H_2O)_{33.25})(Ce_{62}(OH)_{30}(O)_{58}(SO_4)_{72}(H_2O)_{29.75})$, crystallizes in the triclinic space group *P*-1 (V = 58,252 (4) Å^3, **table S3**). The Ce_{62} cluster, formulated $[Ce_{62}(OH)_{30}(O)_{58}(SO_4)_{58}]^{14-}$, is missing a single hexamer and two monomers to complete a full Ce_{70} (**figure 4a**). Addenda sulfates decorate the partially formed rings and serve as interaction points to the neighboring fragments via H-bonding ammoniums. The ring fragments dimerize almost perpendicular to each other, with a 14° torsion between both ends of the fragments (**figure 4b,c**). Ce-O bond distances within Ce_{62} (**table S17**) are comparable with those of Ce_{70} (**table S9**), suggesting the strain of the torsion is delocalized throughout the open ring. The sulfates capping the ring-ends are partially occupied, consistent with lability, allowing completion of the ring under appropriate conditions. The completed Ce_{70} ring with no other building units is obtained as minor co-crystallites along with Ce_{62} crystals, in two different unit cells. See **figures S5,6 and tables S5,6** for additional information.

Pair distribution function (PDF) analysis of the amorphous solid that precipitates upon preparing **$NH_4(Ce_{62})_2$** reaction solutions ($(NH_4)_2SO_4$ plus $Ce(SO_4)_2$) provides compelling evidence that the **Ce_{62}-**ring begins to form immediately upon combining $Ce(SO_4)_2$ plus NH_4^+ (**figure 5b and S13**). Pair correlations out to ~14.5Å are observed and are largely attributable to Ce-Ce pairs due to their high scattering strength compared to other elements present in the material. While this precipitate may be a mixture of the species proposed in this paper, only larger species, such as the **Ce_{62}** or **Ce_{70}** rings or even **Ce_{13}**, have Ce-Ce pairs at this particular distance. The experimental and simulated PDF match well, with the most notable exception being a weaker than expected minor peak just above 6Å that corresponds to Ce-Ce pairs on the inner edge of the ring fragments. This discrepancy may be attributable to a degree of flexibility of this open ring structure at room temperature that broadens the signal at this pair distance. Finally, the scattering spectrum from 5-50º-2θ (Mo-Kα; **figure S13**) presents similar features as the spectrum simulated from the single-crystal structure of **$NH_4(Ce_{62})_2$**. However, diffraction peaks are broader with fewer features in the experimental spectrum than for the calculated spectrum, as expected for a disordered structure.

Considering assembly mechanisms and the role of the ammonium, room temperature SAXS of $Ce(SO_4)_2$ alone suggests it consists of 90% hexamer-sized species, and 10% larger species (**figure 6a**, purple curve), discussed later. This means these small cluster building blocks (Ce_6) assemble immediately from the monomer salt, likely due to Ce^{IV} acidity creating O/OH linkages, as well as the tendency of sulfate ligands to bridge and cap.

Addition of the ammonium as a nitrate salt or acetate salt also produced rapid precipitation, affirming the NH_4^+ is responsible for the rapid assembly of Ce_{62} interlocking rings. Inspecting the **$NH_4(Ce_{62})_2$** structure along with the $Ce(SO_4)_2$ SAXS data (dominated by hexamers) provides compelling evidence that $(Ce_{62})_2$ assembly is initiated at the point of linkage between the two rings. **Figure 5a** highlights this region of the structure, showing the two end-hexamers of one Ce_{62} (maroon) connecting the 5th (central) hexamer in the middle of the adjoining Ce_{62} (blue). Between these three hexamers is a strong H-bonded network of ammonium cations, H_4N—$O_{sulfate}$ or H_4N—

O_{Ce} distances are in the range of 2.7-3.0 Å. There is a similar network between the two end hexamers and the hexamers that flank the central hexamer (4th and 6th) of the adjoining Ce_{62}. In summary, the highlighted area in **figure 5a** is likely the nucleation point of assembly of the interlocking $(Ce_{62})_2$, from the prevalent hexamers. Thus, we hypothesize that Ce_{62} grows symmetrically from either the end hexamers (maroon) or the central hexamer (blue). It is possible that the second connection point of the interlocked $(Ce_{62})_2$ grows simultaneously. Nonetheless, the assembly mechanism, based on the combined solid-state and solution data, is hexamer-by-hexamer addition, but with more complex growth paths than sequential addition around the ring.

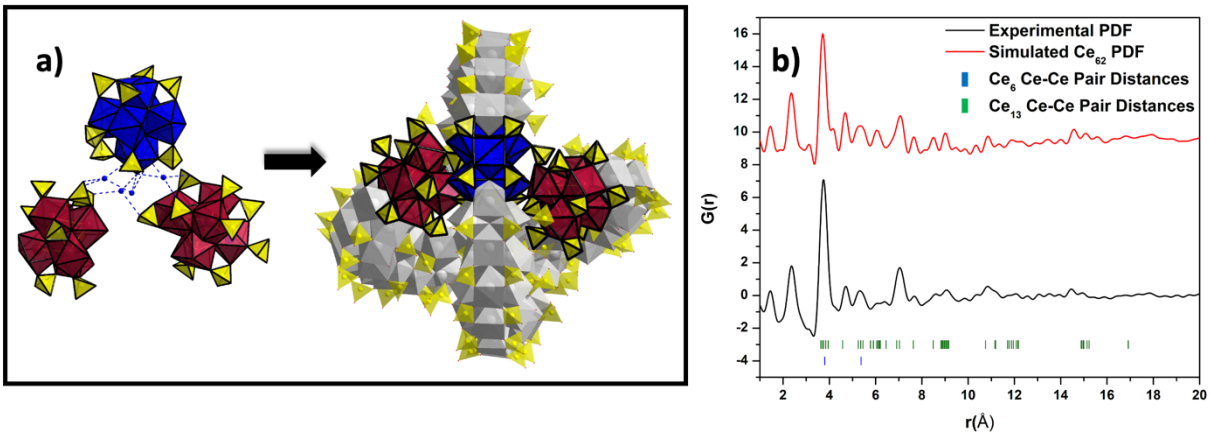

Figure 5. a) Proposed mechanism of $[Ce_{62}]_2$ dimer assembly, templated by ammonium. On the left, three hexamers associate by H-bonding through associated NH_4^+-cations (blue spheres, blue dotted lines show H-bonding, H_4N-$O_{sulfate}$ or H_4N---O_{Ce} distances are in the range of 2.7-3.0 Å). The blue Ce_6 is at the center position (5th hexamer from either open-end) of one Ce_{62}, and the maroon hexamers are the end-caps to the other Ce_{62}. The right is the same Ce_6-hexamers highlighted in the $[Ce_{62}]_2$ dimer. **b)** Simulated PDF for **$NH_4(Ce_{62})_2$** compared to experimental scattering for amorphous $Ce(SO_4)_2$ plus NH_4^+ precipitate. Tick marks at the bottom indicate expected Ce-Ce pair distances in the Ce_6 and Ce_{13} clusters.

Due to the unique synthesis of the ammonium-cerium assemblies, opportunity for synthetic modification emerges after hydrothermal processing but before crystallization of **$NH_4(Ce_{62})_2$**. As previously mentioned, the NH_4^+-Ce^{IV}-SO_4^{2-} solutions crystallize only upon cooling from 75°C to room temperature. At this point we can add heteroatoms to promote framework formation, and we demonstrated this with addition of $CeCl_3$ (see SI). Upon cooling the solution, a new structure crystallized out. The **$NH_4Ce(Ce_{62})_2$**, formulated as $(NH_4)_{71}(Ce_{1.25}(H_2O)_{4.5})$ $(Ce_{62}(OH)_{30}(O)_{58}(SO_4)_{70}(H_2O)_{31.5})$ $(Ce_{62}(OH)_{30}(O)_{58}(SO_4)_{70}(H_2O)_{33.25})$, crystallizes in the triclinic space group *P*-1 (V = 59,403 (8) $Å^3$, **table S4**). The Ce^{III}-monomers are located at two of the four anchor points; one is fully occupied, the second exhibits ¼ occupancy (**figure 4d**). BVA of the monomers confirms these are trivalent (**table S18**).

Tracking Ce_{70} formation in solution

SAXS solution studies tracked formation of Ce_{70} in solution conditions where solubility is maintained, in particular to determine the role of the counter-cation. Single crystal data often

shows only the end result of solution processes; however, SAXS can provide insight into subtle changes in solution. Starting with the same $Ce(SO_4)_2$ solution concentration used for synthesis (0.3 M), cluster growth was promoted by the addition of LiOH (**figure S10**), wherein Li^+ can serve as a counterion and the OH^- can drive hydrolysis. Li^+ was chosen as the counter-cation to support solubility and to minimize competitive X-ray scattering. Even at high acidity and high concentration, dissolved $Ce(SO_4)_2$ shows a high degree of polymerization (discussed below). Increasing the pH from 0.75 (self-buffering) to 1.12, 1.38, and finally 1.70 with LiOH promoted assembly of larger species in solution, indicated by the shifting Guinier region to lower-q. In addition, distinctive features indicative of the Ce_{70} shape and size is seen by the pair of peaks at high q (1.9 $Å^{-1}$and 2.1 $Å^{-1}$), and by the growth of the oscillation around q = 0.3 $Å^{-1}$.[49-52]

To differentiate the effects of increasing pH with increasing counterions, the experiment was repeated using $LiNO_3$ instead of LiOH, and was found to be virtually identical. The $LiNO_3$-$Ce(SO_4)_2$ series is shown in **figure 6a**. Both LiOH and $LiNO_3$ solutions crystallize Li-Ce_{70} directly in the SAXS capillary (**figure 6c**, structure reported below). Consistent with instantaneous $[Ce_{62}]_2$ formation and precipitation, this indicates that 1) Ce_{70} readily forms without forced hydrolysis by adding base or heating; and 2) The main function of the counterion, whether it is ammonium, Ce-monomers, transition metals,[51] or lanthanides (below), is to assemble, connect, and balance the very small charge (-4) of the ring. In fact, all structures produced to date have multiple addenda sulfates to charge balance the multiple polyvalent cations that are framework formers.

Size distribution analyses (**figure 6b**) was performed on the SAXS curves to estimate species size and track their evolution with increasing Li^+. The data is summarized in **table S19**, and scattering curve fits are shown in **figure S11**. The size distribution analysis of simple $Ce(SO_4)_2$ solution suggests that 90% of the dissolved species are the Ce_6-hexamer, ~8% of the species are the approximate size of Ce_{13}, and ~2% are the size of the fully formed Ce_{70} cluster. We do not expect to see a high concentration of Ce_{70} due to its low charge/size and, based on our past experience, we know Ce_{70} is poorly soluble in water. There are likely Ce-monomers present as well, but scattering intensity scales as volume^3 of the scattering species; thus, the minor fraction of larger species dominate the spectra. The intermediate size species (~15-18 Å in diameter) could also be a hexamer flanked by two monomers, Ce_{13} flanked by two monomers, etc. As Li^+ is added, the populations of these three identified specie-sizes does not change significantly. However, each population gets larger in diameter (**figure 6b**). The increase in size of the Ce_6 and Ce_{13}-sized populations is most certainly addition of monomers and hexamers, as a stepwise ring growth. The increase in size is substantial for the Ce_{70} population, ~25%. This could represent a minor amount of offset ring-stacking (**figure S12**) seen in many M_{70} crystal structures,[49-52] as a pre-nucleation process,[50] or ring fragments (Ce_6, Ce_{13}, etc.) assembling neighboring rings from the Ce_{70} 'scaffold'. The small population of Ce_{70} in solution represents equilibrium solubility and suggests formation and crystallization is essentially simultaneous. This is contrary to most POM systems where there is a distinct complete assembly, followed by crystallization.

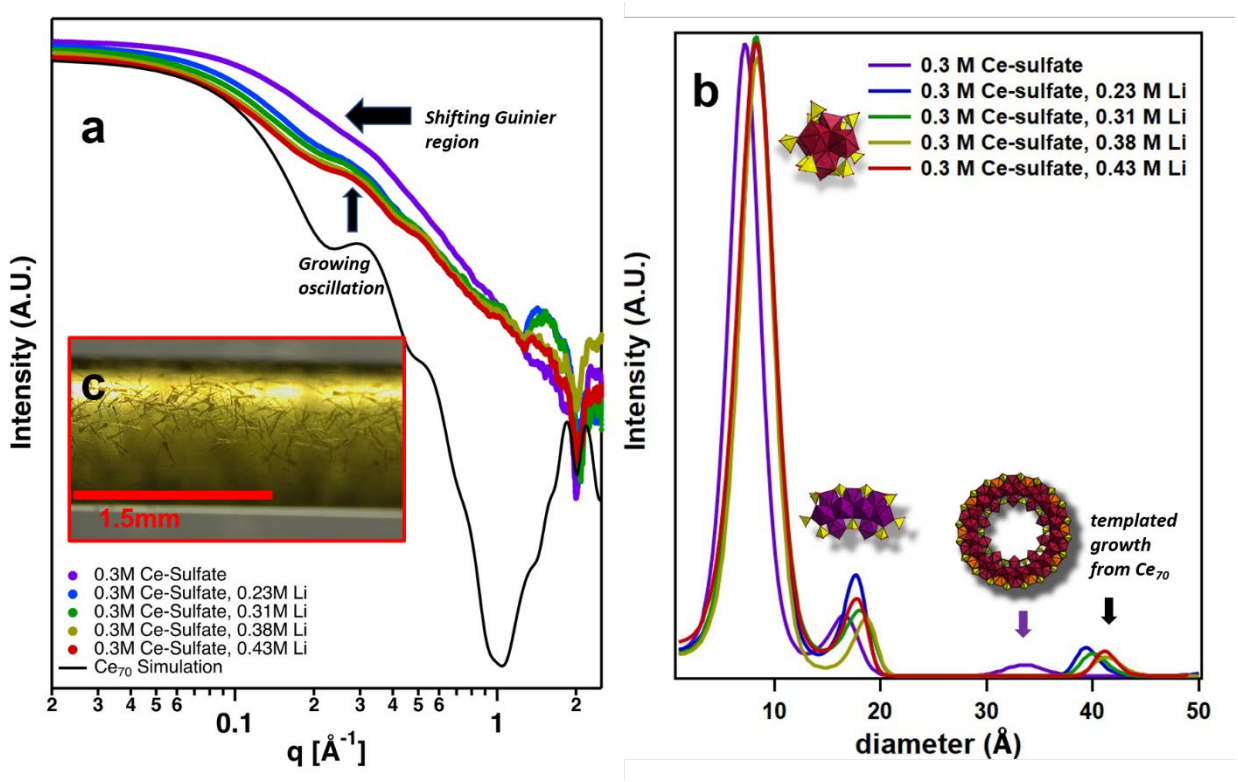

Figure 6. A) Small angle X-ray scatting curves of $Ce(SO_4)_2$ with increasing addition of lithium nitrate. B) Size distribution analyses of the scattering curves that show predominantly Ce_6 hexamers (~90%), species similar in size to Ce_{13} (6-10%), and templated growth off of Ce_{70} (1-3%). C) Microscope image of $LiCe_{70}$ crystals growing inside the SAXS capillary.

Single crystal analysis confirmed the formation of **$LiCe_{70}$** in these experiments. **$LiCe_{70}$** is fully formulated as $Li_{28}Ce_{70}(OH)_{26}(O)_{64}(SO_4)_{77}(H_2O)_{35}$ and crystallizes in the orthorhombic space group *Pnma* (V = 66,045 (11) $Å^3$, **table S7**). In summary, SAXS provides conclusive evidence that the counterions are essential for ring-assembly, and assembly of rings into crystalline lattices.

Ion Sorption and Exchange

We have previously demonstrated that the Ln^{III} are preferentially *absorbed* into $TM^{II}Ce_{70}$ frameworks due to the availability of coordinating sulfates, without evidence for ion exchange except perhaps H_3O^+.[51] However, the role of Ln-counterions in Ce_{70}-framework assembly was not known, nor was the subsequent ion exchange behavior of putative Ln-Ce_{70} frameworks. At the same time, documenting ion exchange behavior of **$NH_4(Ce_{62})_2$** provides further information about this unique phase.

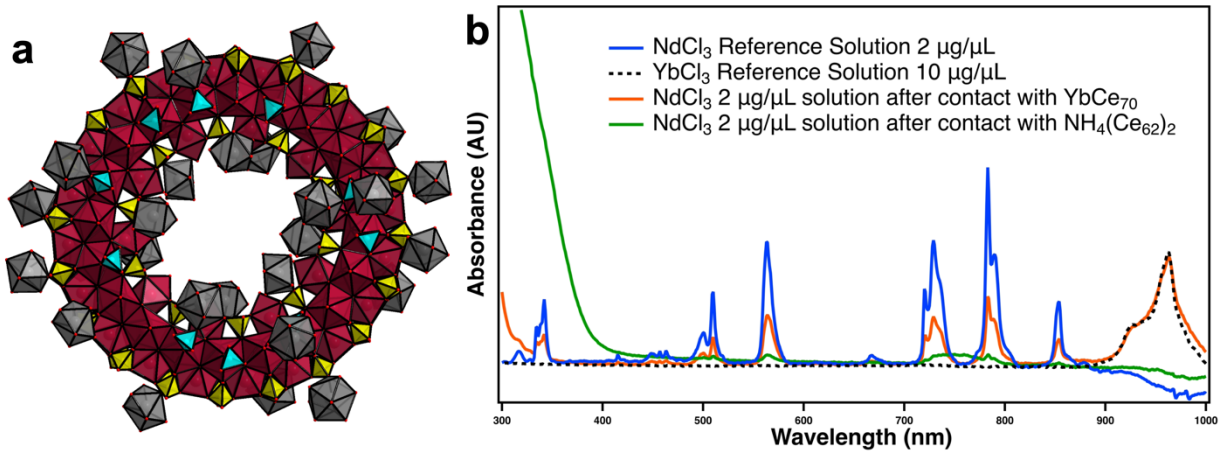

Figure 7. A) Polyhedral Representation of $YbCe_{70}$ showing the Yb monomers in grey, Ce of Ce_{70} in maroon, Ce_{70} sulfates in yellow, addenda sulfates in turquoise and oxygens red. B) UV-VIS spectra of Nd^{3+} solutions before and after contact with $YbCe_{70}$ and $NH_4(Ce_{62})_2$. A Yb^{3+} reference solution confirms ion exchange between Nd and Yb for $YbCe_{70}$.

Adopting the $TM^{II}Ce_{70}$ synthesis to include Yb_2O_3 starting material instead of TM-salts (see SI, synthesis) yielded **$YbCe_{70}$**. This departs from the chemistry of the U^{IV} counterparts. U^{IV} favored U_{70} with transition metals, and the U_{84} 'superatom' with lanthanides.[49] However, given the demonstrated ease of assembly of Ce_{70} in the SAXS study and Ce_{62} with NH_4^+ counterions, it is not surprising that the reaction product is not crucially dependent on the identity of the counter-cation/framework builders (with the exception of ammonium). **$YbCe_{70}$** is fully formulated $Yb_{13}Ce_{70}(OH)_{36}(O)_{64}(SO_4)_{77.5}(H_2O)_{106.5}$ and crystallizes in the triclinic space group *P*-1 (V = 15,499 (2) A^3, **table S8**). The structure reveals Ce_{70} rings stacked in the offset manner, similar to the first row TM^{II} counterparts. Yb^{3+} monomers decorate the inner rim of the ring, bridge the rings stacked along the *a*-axis, and bridge adjacent stacks along the *b*- and *c*-axes (see **figures 7** and **S8**). The Yb-monomers are 8-9 coordinate, with Yb-OSO_3 bond lengths of 2.279 — 2.940 (9) Å and Yb-OH_2 2.218 — 2.579 (7) Å. Additional crystallographic information is compiled in **tables S9,S10**.

Lanthanides, with their distinctive UV-vis spectra, provide a facile method to monitor ion-exchange—both Ln^{3+} that leaves the solution and enters the framework and *vice versa*. This is clearly demonstrated for exchange of Yb^{3+} for Nd^{3+} in the **$YbCe_{70}$** framework (**figure 7b**). The Nd^{3+} peaks are diminished after contact with **$YbCe_{70}$**, and new peaks appear at 963 and 927 nm, consistent with free Yb^{3+} in solution. A titration experiment (**figure S13**) indicates two Yb^{3+} ions per Ce_{70} exchange. Similarly, **$NH_4(Ce_{62})_2$** exchanges in three Nd^{3+} per Ce_{62} (**figure S13**) or six per **$NH_4(Ce_{62})_2$**.

Conclusion

Multiple crystal structures featuring fragments of the Ce_{70}-ring, including a pentamer in a position that indicates templating, provides compelling evidence for a step-wise assembly of the rings. X-ray scattering of amorphous precipitates, along with solution phase scattering, suggests a more

complex mechanism ensues during insipient crystallization, where ring assembly and ordering into a solid-state lattice occurs simultaneously. While transition metal, alkali, and lanthanide cations join the anionic Ce_{70}-rings into frameworks via bridging sulfates, their role in assembly is otherwise minimal, and perhaps the rings could be isolated without counter-cations, as was demonstrated with Zr_{70}.[52] The exceptional counter-cation is ammonium; in its presence, an interlocking dimer of Ce_{62} ring fragments assembles and precipitates spontaneously at room temperature. We have proposed a mechanism of nucleation and growth from the two open ends of the ring towards the middle, based on mutual templating and strong NH_4^+ H-bonding within the dimer. Facile rare earth ion exchange was demonstrated with both Ce_{70} and Ce_{62} phases. We believe the amorphous NH_4^+-Ce_{62}, very easily synthesized, will provide even better ion exchange properties (kinetics and capacity) that could also engage $Ce^{III/IV}$ redox activity. We intend to study this in the future for exchange of rare earth metals, actinides, and specific radionuclides of concern (i.e., ^{137}Cs, ^{90}Sr).

Acknowledgments

This work was supported by the Department of Energy, National Nuclear Security Administration (NNSA) under Award Number DE-NA0003763. We acknowledge the Murdock Charitable Trust (Grant No. SR-2017297) for acquisition of the single-crystal X-ray diffractometer.

References

1. Douglas, S. M.; Dietz, H.; Liedl, T.; Högberg, B.; Graf, F.; Shih, W. M., Self-assembly of DNA into nanoscale three-dimensional shapes. *Nature* **2009,** *459* (7245), 414-418.
2. Pérez-Romero, A.; Domínguez-Martín, A.; Galli, S.; Santamaría-Díaz, N.; Palacios, O.; Dobado, J. A.; Nyman, M.; Galindo, M. A., Single-stranded DNA as supramolecular template for one-dimensional palladium(II) arrays. *Angewandte Chemie International Edition* **2021,** *n/a* (n/a).
3. Whaley, S. R.; English, D. S.; Hu, E. L.; Barbara, P. F.; Belcher, A. M., Selection of peptides with semiconductor binding specificity for directed nanocrystal assembly. *Nature* **2000,** *405* (6787), 665-668.
4. Gazit, E., Self-assembled peptide nanostructures: the design of molecular building blocks and their technological utilization. *Chemical Society Reviews* **2007,** *36* (8), 1263.
5. Mal, S. S.; Kortz, U., The Wheel-Shaped Cu20 Tungstophosphate [Cu20Cl(OH)24(H2O)12(P8W48O184)]25− Ion. *Angewandte Chemie International Edition* **2005,** *44* (24), 3777-3780.
6. Mal, S. S.; Nsouli, N. H.; Dickman, M. H.; Kortz, U., Organoruthenium derivative of the cyclic [H7P8W48O184]33? anion: [{K(H2O)}3{Ru(p-cymene)(H2O)}4P8W49O186(H2O)2]27? *Dalton Transactions* **2007,** (25), 2627.
7. Mitchell, S. G.; Gabb, D.; Ritchie, C.; Hazel, N.; Long, D.-L.; Cronin, L., Controlling nucleation of the cyclic heteropolyanion {P8W48}: a cobalt-substituted phosphotungstate chain and network. *CrystEngComm* **2009,** *11* (1), 36-39.
8. Mitchell, S. G.; Streb, C.; Miras, H. N.; Boyd, T.; Long, D.-L.; Cronin, L., Face-directed self-assembly of an electronically active Archimedean polyoxometalate architecture. *Nature Chemistry* **2010,** *2* (4), 308-312.
9. Mitchell, S. G.; Boyd, T.; Miras, H. N.; Long, D.-L.; Cronin, L., Extended Polyoxometalate Framework Solids: Two Mn(II)-Linked {P8W48} Network Arrays. *Inorganic Chemistry* **2011,** *50* (1), 136-143.
10. Cavka, J. H.; Jakobsen, S.; Olsbye, U.; Guillou, N.; Lamberti, C.; Bordiga, S.; Lillerud, K. P., A New Zirconium Inorganic Building Brick Forming Metal Organic Frameworks with Exceptional Stability. *Journal of the American Chemical Society* **2008,** *130* (42), 13850-13851.
11. Lammert, M.; Wharmby, M. T.; Smolders, S.; Bueken, B.; Lieb, A.; Lomachenko, K. A.; Vos, D. D.; Stock, N., Cerium-based metal organic frameworks with UiO-66 architecture: synthesis, properties and redox catalytic activity. *Chemical Communications* **2015,** *51* (63), 12578-12581.
12. Zhang, J.-P.; Huang, X.-C.; Chen, X.-M., Supramolecular isomerism in coordination polymers. *Chemical Society Reviews* **2009,** *38* (8), 2385.
13. Chen, R.; Yan, Z. H.; Kong, X. J.; Long, L. S.; Zheng, L. S., Integration of Lanthanide–Transition-Metal Clusters onto CdS Surfaces for Photocatalytic Hydrogen Evolution. *Angewandte Chemie International Edition* **2018,** *57* (51), 16796-16800.
14. Jamet, M.; Wernsdorfer, W.; Thirion, C.; Mailly, D.; Dupuis, V.; Mélinon, P.; Pérez, A., Magnetic Anisotropy of a Single Cobalt Nanocluster. *Physical Review Letters* **2001,** *86* (20), 4676-4679.
15. Kong, X.-J.; Ren, Y.-P.; Long, L.-S.; Zheng, Z.; Huang, R.-B.; Zheng, L.-S., A Keplerate Magnetic Cluster Featuring an Icosidodecahedron of Ni(II) Ions Encapsulating a Dodecahedron of La(III) Ions. *Journal of the American Chemical Society* **2007,** *129* (22), 7016-7017.
16. Cremades, E.; Gómez-Coca, S.; Aravena, D.; Alvarez, S.; Ruiz, E., Theoretical Study of Exchange Coupling in 3d-Gd Complexes: Large Magnetocaloric Effect Systems. *Journal of the American Chemical Society* **2012,** *134* (25), 10532-10542.
17. Peng, J.-B.; Zhang, Q.-C.; Kong, X.-J.; Ren, Y.-P.; Long, L.-S.; Huang, R.-B.; Zheng, L.-S.; Zheng, Z., A 48-Metal Cluster Exhibiting a Large Magnetocaloric Effect. *Angewandte Chemie International Edition* **2011,** *50* (45), 10649-10652.

18. Peng, J.-B.; Kong, X.-J.; Zhang, Q.-C.; Orendáč, M.; Prokleška, J.; Ren, Y.-P.; Long, L.-S.; Zheng, Z.; Zheng, L.-S., Beauty, Symmetry, and Magnetocaloric Effect—Four-Shell Keplerates with 104 Lanthanide Atoms. *Journal of the American Chemical Society* **2014,** *136* (52), 17938-17941.
19. Yang, X.; Schipper, D.; Jones, R. A.; Lytwak, L. A.; Holliday, B. J.; Huang, S., Anion-Dependent Self-Assembly of Near-Infrared Luminescent 24- and 32-Metal Cd–Ln Complexes with Drum-like Architectures. *Journal of the American Chemical Society* **2013,** *135* (23), 8468-8471.
20. Zhang, Q.; Lei, M.; Yan, H.; Wang, J.; Shi, Y., A Water-Stable 3D Luminescent Metal−Organic Framework Based on Heterometallic [EuIII6ZnII] Clusters Showing Highly Sensitive, Selective, and Reversible Detection of Ronidazole. *Inorganic Chemistry* **2017,** *56* (14), 7610-7614.
21. Christie, L. G.; Surman, A. J.; Scullion, R. A.; Xu, F.; Long, D.-L.; Cronin, L., Overcoming the Crystallization Bottleneck: A Family of Gigantic Inorganic {Pd x }L (x= 84, 72) Palladium Macrocycles Discovered using Solution Techniques. *Angewandte Chemie* **2016,** *128* (41), 12933-12937.
22. Scullion, R. A.; Surman, A. J.; Xu, F.; Mathieson, J. S.; Long, D.-L.; Haso, F.; Liu, T.; Cronin, L., Exploring the Symmetry, Structure, and Self-Assembly Mechanism of a Gigantic Seven-Fold Symmetric {Pd84} Wheel. *Angewandte Chemie International Edition* **2014,** *53* (38), 10032-10037.
23. Xu, F.; Miras, H. N.; Scullion, R. A.; Long, D. L.; Thiel, J.; Cronin, L., Correlating the magic numbers of inorganic nanomolecular assemblies with a molecular-ring Rosetta Stone. *Proceedings of the National Academy of Sciences* **2012,** *109* (29), 11609-11612.
24. Tasiopoulos, A. J.; Vinslava, A.; Wernsdorfer, W.; Abboud, K. A.; Christou, G., Giant Single-Molecule Magnets: A{Mn84} Torus and Its Supramolecular Nanotubes. *Angewandte Chemie* **2004,** *116* (16), 2169-2173.
25. Vinslava, A.; Tasiopoulos, A. J.; Wernsdorfer, W.; Abboud, K. A.; Christou, G., Molecules at the Quantum–Classical Nanoparticle Interface: Giant Mn70 Single-Molecule Magnets of ∼4 nm Diameter. *Inorganic Chemistry* **2016,** *55* (7), 3419-3430.
26. Liu, T.; Diemann, E.; Li, H.; Dress, A. W. M.; Müller, A., Self-assembly in aqueous solution of wheel-shaped Mo154 oxide clusters into vesicles. *Nature* **2003,** *426* (6962), 59-62.
27. Müller, A.; Krickemeyer, E.; Meyer, J.; Bögge, H.; Peters, F.; Plass, W.; Diemann, E.; Dillinger, S.; Nonnenbruch, F.; Randerath, M.; Menke, C., [Mo154(NO)14O420(OH)28(H2O)70](25± 5)−: A Water-Soluble Big Wheel with More than 700 Atoms and a Relative Molecular Mass of About 24000. *Angewandte Chemie International Edition in English* **1995,** *34* (19), 2122-2124.
28. Wang, R.; Liu, H.; Carducci, M. D.; Jin, T.; Zheng, C.; Zheng, Z., Lanthanide Coordination with α-Amino Acids under Near Physiological pH Conditions: Polymetallic Complexes Containing the Cubane-Like [Ln4(μ3-OH)4]8+Cluster Core. *Inorganic Chemistry* **2001,** *40* (12), 2743-2750.
29. Wang, R.; Selby, H. D.; Liu, H.; Carducci, M. D.; Jin, T.; Zheng, Z.; Anthis, J. W.; Staples, R. J., Halide-Templated Assembly of Polynuclear Lanthanide-Hydroxo Complexes†. *Inorganic Chemistry* **2002,** *41* (2), 278-286.
30. Kong, X.-J.; Wu, Y.; Long, L.-S.; Zheng, L.-S.; Zheng, Z., A Chiral 60-Metal Sodalite Cage Featuring 24 Vertex-Sharing [Er4(μ3-OH)4] Cubanes. *Journal of the American Chemical Society* **2009,** *131* (20), 6918-6919.
31. Zheng, X.-Y.; Jiang, Y.-H.; Zhuang, G.-L.; Liu, D.-P.; Liao, H.-G.; Kong, X.-J.; Long, L.-S.; Zheng, L.-S., A Gigantic Molecular Wheel of {Gd140}: A New Member of the Molecular Wheel Family. *Journal of the American Chemical Society* **2017,** *139* (50), 18178-18181.
32. Li, S.-R.; Wang, H.-Y.; Su, H.-F.; Chen, H.-J.; Du, M.-H.; Long, L.-S.; Kong, X.-J.; Zheng, L.-S., A Giant 3d-4f Polyoxometalate Super-Tetrahedron with High Proton Conductivity. *Small Methods* **2020,** *n/a* (n/a), 2000777.
33. Du, M.-H.; Zheng, X.-Y.; Kong, X.-J.; Long, L.-S.; Zheng, L.-S., Synthetic Protocol for Assembling Giant Heterometallic Hydroxide Clusters from Building Blocks: Rational Design and Efficient Synthesis. *Matter* **2020,** *3* (4), 1334-1349.

34. Hou, Y.; Zakharov, L. N.; Nyman, M., Observing Assembly of Complex Inorganic Materials from Polyoxometalate Building Blocks. *Journal of the American Chemical Society* **2013,** *135* (44), 16651-16657.
35. Zhang, G. Y.; Gadot, E.; Gan-Or, G.; Baranov, M.; Tubul, T.; Neyman, A.; Li, M.; Clotet, A.; Poblet, J. M.; Yin, P. C.; Weinstock, I. A., Self-Assembly and Ionic-Lattice-like Secondary Structure of a Flexible Linear Polymer of Highly Charged Inorganic Building Blocks. *Journal of the American Chemical Society* **2020,** *142* (16), 7295-7300.
36. Chen, L.; Turo, M. J.; Gembicky, M.; Reinicke, R. A.; Schimpf, A. M., Cation-Controlled Assembly of Polyoxotungstate-Based Coordination Networks. *Angewandte Chemie International Edition* **2020**.
37. Bai, Y.; Dou, Y. B.; Xie, L. H.; Rutledge, W.; Li, J. R.; Zhou, H. C., Zr-based metal-organic frameworks: design, synthesis, structure, and applications. *Chemical Society Reviews* **2016,** *45* (8), 2327-2367.
38. Dufaye, M.; Martin, N. P.; Duval, S.; Volkringer, C.; Ikeda-Ohno, A.; Loiseau, T., Time-controlled synthesis of the 3D coordination polymer U(1,2,3-Hbtc)2 followed by the formation of molecular poly-oxo cluster {U14} containing hemimellitate uranium(iv). *RSC Advances* **2019,** *9* (40), 22795-22804.
39. Falaise, C.; Volkringer, C.; Vigier, J.-F.; Beaurain, A.; Roussel, P.; Rabu, P.; Loiseau, T., Isolation of the Large {Actinide}38 Poly-oxo Cluster with Uranium. *Journal of the American Chemical Society* **2013,** *135* (42), 15678-15681.
40. Martin, N. P.; Volkringer, C.; Henry, N.; Trivelli, X.; Stoclet, G.; Ikeda-Ohno, A.; Loiseau, T., Formation of a new type of uranium(iv) poly-oxo cluster {U38} based on a controlled release of water via esterification reaction. *Chemical Science* **2018,** *9* (22), 5021-5032.
41. Martin, N. P.; Volkringer, C.; Roussel, P.; März, J.; Hennig, C.; Loiseau, T.; Ikeda-Ohno, A., {Np38} clusters: the missing link in the largest poly-oxo cluster series of tetravalent actinides. *Chemical Communications* **2018,** *54* (72), 10060-10063.
42. Sigmon, G. E.; Hixon, A. E., Extension of the Plutonium Oxide Nanocluster Family to Include {Pu 16 } and {Pu 22 }. *Chemistry – A European Journal* **2019,** *25* (10), 2463-2466.
43. Vanagas, N. A.; Higgins, R. F.; Wacker, J. N.; Asuigui, D. R. C.; Warzecha, E.; Kozimor, S. A.; Stoll, S. L.; Schelter, E. J.; Bertke, J. A.; Knope, K. E., Mononuclear to Polynuclear U IV Structural Units: Effects of Reaction Conditions on U-Furoate Phase Formation. *Chemistry – A European Journal* **2020,** *26* (26), 5872-5886.
44. Mitchell, K. J.; Goodsell, J. L.; Russell-Webster, B.; Twahir, U. T.; Angerhofer, A.; Abboud, K. A.; Christou, G., Expansion of the Family of Molecular Nanoparticles of Cerium Dioxide and Their Catalytic Scavenging of Hydroxyl Radicals. *Inorganic Chemistry* **2021,** *60* (3), 1641-1653.
45. Falaise, C.; Kozma, K.; Nyman, M., Thorium Oxo-Clusters as Building Blocks for Open Frameworks. *Chemistry – A European Journal* **2018,** *24* (53), 14226-14232.
46. Colliard, I.; Falaise, C.; Nyman, M., Bridging the Transuranics with Uranium(IV) Sulfate Aqueous Species and Solid Phases. *Inorganic Chemistry* **2020,** *59* (23), 17049-17057.
47. Mitchell, K. J.; Abboud, K. A.; Christou, G., Atomically-precise colloidal nanoparticles of cerium dioxide. *Nature Communications* **2017,** *8* (1).
48. Wasson, M. C.; Zhang, X.; Otake, K.-I.; Rosen, A. S.; Alayoglu, S.; Krzyaniak, M. D.; Chen, Z.; Redfern, L. R.; Robison, L.; Son, F. A.; Chen, Y.; Islamoglu, T.; Notestein, J. M.; Snurr, R. Q.; Wasielewski, M. R.; Farha, O. K., Supramolecular Porous Assemblies of Atomically Precise Catalytically Active Cerium-Based Clusters. *Chemistry of Materials* **2020,** *32* (19), 8522-8529.
49. Colliard, I.; Morrison, G.; Loye, H.-C. Z.; Nyman, M., Supramolecular Assembly of U(IV) Clusters and Superatoms with Unconventional Countercations. *Journal of the American Chemical Society* **2020,** *142* (19), 9039-9047.
50. Colliard, I.; Nyman, M., Building [U IV 70 (OH) 36 (O) 64] 4− Oxocluster Frameworks with Sulfate, Transition Metals, and U V. *Chemistry – A European Journal* **2020,** *26* (54), 12481-12488.
51. Colliard, I.; Nyman, M., CeIV70 oxosulfate rings, frameworks, supramolecular assembly and redox activity. *Angewandte Chemie International Edition* **2021**.

52. Øien-Ødegaard, S.; Bazioti, C.; Redekop, E. A.; Prytz, Ø.; Lillerud, K. P.; Olsbye, U., A Toroidal Zr 70 Oxysulfate Cluster and Its Diverse Packing Structures. *Angewandte Chemie International Edition* **2020,** *59* (48), 21397-21402.
53. Miras, H. N.; Cooper, G. J. T.; Long, D. L.; Bogge, H.; Muller, A.; Streb, C.; Cronin, L., Unveiling the Transient Template in the Self-Assembly of a Molecular Oxide Nanowheel. *Science* **2010,** *327* (5961), 72-74.
54. Wang, W.; Fullmer, L. B.; Bandeira, N. A. G.; Goberna-Ferrón, S.; Zakharov, L. N.; Bo, C.; Keszler, D. A.; Nyman, M., Crystallizing Elusive Chromium Polycations. *Chem* **2016,** *1* (6), 887-901.
55. Wang, W.; Wentz, K. M.; Hayes, S. E.; Johnson, D. W.; Keszler, D. A., Synthesis of the Hydroxide Cluster [Al13(µ3-OH)6(µ-OH)18(H2O)24]15+ from an Aqueous Solution. *Inorganic Chemistry* **2011,** *50* (11), 4683-4685.
56. Casey, W. H., Large Aqueous Aluminum Hydroxide Molecules. *Chemical Reviews* **2006,** *106* (1), 1-16.
57. Shohel, M.; Bjorklund, J. L.; Smith, J. A.; Kravchuk, D. V.; Mason, S. E.; Forbes, T. Z., Formation of Nanoscale [Ge4O16Al48(OH)108(H2O)24]20+ from Condensation of ϵ-GeAl128+ Keggin Polycations**. *Angewandte Chemie International Edition* **2021,** *60* (16), 8755-8759.
58. Misra, A.; Kozma, K.; Streb, C.; Nyman, M., Beyond Charge Balance: Counter-Cations in Polyoxometalate Chemistry. *Angewandte Chemie International Edition* **2020,** *59* (2), 596-612.
59. Henry, M.; Jolivet, J. P.; Livage, J., Aqueous chemistry of metal cations: Hydrolysis, condensation and complexation. In *Chemistry, Spectroscopy and Applications of Sol-Gel Glasses*, Reisfeld, R.; Jjørgensen, C. K., Eds. Springer Berlin Heidelberg: Berlin, Heidelberg, 1992; pp 153-206.
60. Ray, D.; Xie, J.; White, J.; Sigmon, G. E.; Gagliardi, L.; Hixon, A. E., Experimental and Quantum Mechanical Characterization of an Oxygen-Bridged Plutonium(IV) Dimer. *Chemistry – A European Journal* **2020,** *26* (36), 8115-8120.
61. Sidey, V., On the effective ionic radii for ammonium. *Acta Crystallographica Section B* **2016,** *72* (4), 626-633.